Cinacalcet corrects hypercalcemia in mice with an inactivating $G\alpha_{11}$ mutation

Sarah A. Howles[1], Fadil M. Hannan[1,2], Caroline M. Gorvin[1], Sian E. Piret[1], Anju Paudyal[3], Michelle Stewart[3], Tertius A. Hough[3], M. Andrew Nesbit[1,4], Sara Wells[3], Stephen D. M. Brown[3], Roger D. Cox[3], Rajesh V. Thakker[1]

Authorship note: Sarah Howles, Fadil Hannan and Caroline Gorvin contributed equally to this work

[1]Academic Endocrine Unit, Radcliffe Department of Medicine, University of Oxford, Oxford, UK. [2]Department of Musculoskeletal Biology, Institute of Ageing and Chronic Disease, University of Liverpool, Liverpool, UK. [3]Mammalian Genetics Unit and Mary Lyon Centre, MRC Harwell Institute, Harwell Science and Innovation Campus, UK. [4]Biomedical Sciences Research Institute, Ulster University, Coleraine, UK.

Address correspondence to: Rajesh V. Thakker at the Academic Endocrine Unit, Radcliffe Department of Medicine, Oxford Centre for Diabetes, Endocrinology and Metabolism (OCDEM), Churchill Hospital, Oxford OX3 7LJ, United Kingdom. Tel no: 01865 857501. Fax no: 01865 875502. Email: rajesh.thakker@ndm.ox.ac.uk.

Conflict of interest: F.M.H and R.V.T. have received grant funding from NPS/Shire Pharmaceuticals and GlaxoSmithKline for studies involving the use of calcium-sensing receptor (CaSR) allosteric inhibitors. R.V.T. has also received grants from Novartis Pharma AG and the Marshall Smith Syndrome Foundation for unrelated studies. S.D.M.B. declares ownership of shares in Pulmagen Therapeutics.

Manuscript word count = 7635 (limit =12000 words)

Abstract

Loss-of-function mutations of *GNA11*, which encodes G-protein subunit α_{11} ($G\alpha_{11}$), a signaling partner for the calcium-sensing receptor (CaSR), result in familial hypocalciuric hypercalcemia type 2 (FHH2). FHH2 is characterized by hypercalcemia, inappropriately normal or raised PTH concentrations, and normal or low urinary calcium excretion. A mouse model for FHH2 which would facilitate investigations of the *in vivo* role of $G\alpha_{11}$ and the evaluation of calcimimetic drugs, that are CaSR allosteric activators, is not available. We therefore screened DNA from >10,000 mice treated with the chemical mutagen *N*-ethyl-*N*-nitrosourea (ENU) for *Gna11* mutations, and identified a $G\alpha_{11}$ variant, Asp195Gly (D195G), which *in vitro* down-regulated CaSR-mediated intracellular calcium signaling, consistent with it being a loss-of-function mutation. Treatment with the calcimimetic cinacalcet rectified these signaling responses. *In vivo* studies showed mutant heterozygous (*Gna11*$^{+/195G}$) and homozygous (*Gna11*$^{195G/195G}$) mice to be hypercalcemic with normal or increased plasma PTH concentrations, and normal urinary calcium excretion. Cinacalcet (30mg/kg orally) significantly reduced plasma albumin-adjusted calcium and PTH concentrations in *Gna11*$^{+/195G}$ and *Gna11*$^{195G/195G}$ mice. Thus, our studies have established a mouse model with a germline loss-of-function $G\alpha_{11}$ mutation, that is representative for FHH2 in humans, and demonstrated that cinacalcet can correct the associated abnormalities of plasma calcium and PTH.

Introduction

Familial hypocalciuric hypercalcemia (FHH) is an autosomal dominant disorder of extracellular calcium (Ca^{2+}_o) homeostasis characterized by lifelong elevations in serum calcium concentrations in association with normal or mildly elevated serum parathyroid hormone (PTH) concentrations, and normal or low fractional excretion of calcium (1-4). FHH is caused by a reduction in the sensitivity of the Ca^{2+}_o-sensing receptor (CaSR) signaling pathway to alterations in the prevailing Ca^{2+}_o concentration ($[Ca^{2+}]_o$) (1-4). The CaSR is a widely expressed family C G-protein coupled receptor (GPCR) that regulates PTH secretion and urinary calcium excretion by transducing elevations in $[Ca^{2+}]_o$ into multiple intracellular signaling cascades in the parathyroid glands and kidneys, respectively (5, 6). In the parathyroid glands, the CaSR has been shown to couple to the $G_{q/11}$ protein family (7), which activates phospholipase C (PLC), thereby increasing intracellular calcium (Ca^{2+}_i) and mitogen-activated protein kinase (MAPK) signaling responses (8, 9), which in turn leads to decreased parathyroid PTH secretion.

FHH is a genetically heterogeneous disorder with three recognized forms referred to as FHH types 1-3 (FHH1-3) (1). FHH1 (OMIM #145980) is caused by heterozygous loss-of-function mutations of the CaSR, which is encoded by the *CASR* gene on chromosome 3q21.1 (1). FHH2 (OMIM #145981) is due to heterozygous loss-of-function mutations of G-protein subunit α_{11} ($G\alpha_{11}$), which is encoded by the *GNA11* gene on chromosome 19p13.3, and to date, three FHH2-associated mutations have been reported, comprising two missense mutations, Thr54Met and Leu135Gln, and an in-frame isoleucine deletion at codon 200 (Ile200del) (3, 10). FHH3 (OMIM #600740) is caused by heterozygous loss-of-function mutations of the adaptor protein-2 σ subunit (AP2σ), encoded by the *AP2S1* gene on chromosome 19q13.3, which is involved in the clathrin-mediated endocytosis of cell-surface proteins such as the CaSR (4, 11).

A mouse model for FHH1 has previously been generated by targeted germline disruption of the *Casr* gene, and heterozygous ($Casr^{+/-}$) mice were shown to have a phenotype resembling that of FHH1 patients with elevated serum concentrations of calcium and PTH, and low urinary calcium excretion (12). In addition, homozygous ($Casr^{-/-}$) mice had features of neonatal severe

hyperparathyroidism (NSHPT), which is caused by biallelic inactivating CaSR mutations (1), and exhibited growth retardation and died within the first 30 days of life (12). An *in vivo* model is not available for FHH2, although mice with parathyroid-specific combined ablations of both the *Gna11* and *Gnaq* (encoding $G\alpha_q$) genes have previously been reported to develop marked hypercalcemia and hyperparathyroidism (7). We therefore sought to establish a mouse model for FHH2 to define the *in vivo* role of $G\alpha_{11}$ in Ca^{2+}_o homeostasis, and to undertake a more detailed characterization of the phenotype of this disorder, as limited information is available from the few FHH2 patients reported to date (3, 10). In addition, a mouse model for FHH2 would facilitate evaluation of therapeutic drugs such as CaSR allosteric activators, also known as calcimimetics (13). To establish a mouse model for FHH2, due to a germline loss-of-function *GNA11* point mutation (3, 10), we screened a DNA archive of >10,000 samples from male mice that had mutations induced by treating them with *N*-ethyl-*N*-nitrosourea (ENU), a chemical mutagen. ENU is an alkylating agent that introduces point mutations via transfer of an alkyl group from ENU to a DNA base, thus leading to mispairing and base pair substitution during subsequent DNA replication (14, 15). ENU mutagenesis programs utilize two complementary approaches that are phenotype-driven and genotype-driven screens. In phenotype-driven screens, offspring of mutagenized mice are assessed for abnormalities in a hypothesis-generating strategy, which may elucidate new genes, pathways, and mechanisms for disease phenotypes (14, 15). Genotype-driven screens in which mutations in the gene of interest are sought are hypothesis-driven and are feasible by available parallel archives of tissue-DNA and sperm samples from mutagenized male mice (14, 15). The archived tissue-DNA samples from the mutagenized male mice are used to search for the mutations in the gene of interest, and once these mutations are found, then a sperm sample from the male mouse with the mutation is used for *in vitro* fertilization (IVF) of normal female mice to establish progeny with the mutation (14, 15). The probability of finding three or more variant alleles in an archive of tissue-DNA samples from >5000 ENU-mutagenized mice is >90% (14). We sought for ENU-induced *Gna11* variants in tissue-DNA samples from >10,000 male mice treated with ENU, with the aim of establishing a mouse model for FHH2.

Results

Identification and analysis of five Gna11 variants in ENU-mutagenized mice. An analysis using melting curve analysis (16) of tissue-DNA samples from >10,000 ENU-mutagenized male mice, of the seven exons and 12 intron-exon boundaries of the *Gna11* gene revealed the presence of five *Gna11* variants, comprising c.621C>T, c.637T>A, c.682G>A, c.826A>g, and c.1048T>C (Supplementary Table 1). These five *Gna11* variants predicted the occurrence of 4 missense variants (Ile132Asn, Arg147His, Asp195Gly and Val269Ala) and one nonsense variant (Gln127Stop) (Figure 1A and Supplementary Figure 1). Bioinformatic analysis predicted all the $G\alpha_{11}$ variants to be damaging and likely disease-causing (Supplementary Table 1). FHH2 has been reported to be caused by either an in-frame deletion or missense substituitions affecting $G\alpha_{11}$ (3, 10) and we therefore further characterised only the four missense $G\alpha_{11}$ variants identified in ENU-mutagenized mice. All of these 4 missense variants affected evolutionary conserved residues (Figure 1B, Supplementary Table 1 and Supplementary Figure 1) and two variants (Asp195Gly and Val269Ala) were located in the $G\alpha_{11}$ GTPase domain, which mediates GPCR binding, guanosine triphosphate (GTP) hydrolysis, and effector coupling; and the other two variants (Ile132Asn and Arg147His) were located in the $G\alpha_{11}$ helical domain, which stabilises guanine nucleotide binding (Figure 1A and Supplementary Figure 1) (17). Three-dimensional modeling using the reported crystal structure of the related $G\alpha_q$ protein (18) predicted the Asp195Gly variant to disrupt polar contacts within the $G\alpha_{11}$ GTPase domain (Figure 1C and D), whereas the other missense variants were not predicted to alter intramolecular interactions within the $G\alpha_{11}$ protein (Supplementary Figure 1). We therefore selected the Asp195Gly (D195G) variant for functional characterization for the following four reasons. First, this variant is located within the switch regions of the $G\alpha_{11}$ GTPase domain (Figure 1B and C), which are critical for mediating Gα-subunit conformational changes upon GTP binding, and also for coupling to downstream effector proteins such as PLC (19, 20). Second, the Asp195Gly variant is situated within a 13 amino acid region (residues 193-205), which links switches I and II (Figure 1B and C), and is the location of a reported FHH2-causing $G\alpha_{11}$ mutation (Ile200del) (3). Third, this 13 amino acid linker region also contains the tetrapeptide β2-β3 loop (residues 196-199), which mediates G-protein-GPCR

interactions (21) (Figure 1C), and our reported mutagenesis studies have shown that disruption of the $G\alpha_{11}$ β2-β3 loop impairs signalling in CaSR-expressing cells (3). Fourth, three-dimensional modeling of the Asp195Gly $G\alpha_{11}$ variant predicted that substitution of the WT Asp195 residue with the variant Gly195 residue would lead to a loss of a polar contact within the $G\alpha_{11}$ β2-β3 loop, which would likely disrupt this tetrapeptide loop (Figure 1D), and thereby impair GPCR binding and $G\alpha_{11}$ activation (3, 19, 20). These combined observations indicated that the Asp195Gly variant was highly likely to be a pathogenic mutation.

In vitro functional characterization of the Asp195Gly $G\alpha_{11}$ mutation. To investigate the effects of these predicted $G\alpha_{11}$ structural changes due to the Asp195Gly mutation on CaSR-mediated signaling, human embryonic kidney (HEK) 293 cells stably expressing the CaSR (HEK-CaSR) were transiently transfected with pBI-CMV2-*GNA11-GFP* constructs expressing either the WT (Asp195) or variant (Gly195) $G\alpha_{11}$ proteins, as reported (3). This bidirectional pBI-CMV2 vector allows for co-expression of $G\alpha_{11}$ and GFP at equivalent levels (3). Expression of the CaSR, $G\alpha_{11}$, and GFP was confirmed by fluorescence microscopy and/or Western blot analyses (Figure 2A and B). The expression of $G\alpha_{11}$ was shown to be similar in cells transiently transfected with WT or mutant proteins and to be greater than that observed in untransfected cells (Figure 2B). Moreover, the expression of mutant $G\alpha_{11}$ in cells that endogenously express WT $G\alpha_{11}$ (Figure 2B), corresponded to the heterozygous situation reported in FHH2 patients (3, 10). The $Ca^{2+}{}_i$ responses to alterations in $[Ca^{2+}]_o$ of cells expressing the different *GNA11* vectors were assessed using a multi-well assay that utilized the Fluo-4 Ca^{2+}-binding dye, as reported (22). The $Ca^{2+}{}_i$ responses were shown to increase in a dose-dependent manner following stimulation with increasing $[Ca^{2+}]_o$ (Figure 2C). However, responses in mutant Gly195-expressing cells were significantly decreased compared with WT-expressing cells. (Figure 2C). Thus, the mutant Gly195-expressing cells showed a rightward shift in the concentration-response curve (Figure 2C), with a significantly increased mean half-maximal response (EC_{50}) of 3.39mM (95% confidence interval (CI), 3.26-3.53) compared to 2.70mM (95% CI, 2.53-2.88) for WT (Asp195) expressing cells ($p<0.0001$) (Figure 2C and D). These results demonstrated that the $G\alpha_{11}$ Asp195Gly mutation is a loss-of-function mutation, similar to mutations that lead to FHH2 (3, 10). We next

investigated the ability of the CaSR allosteric activator, cinacalcet, to rectify this loss-of-function associated with the Asp195Gly $G\alpha_{11}$ mutation. Cinacalcet was added to Gly195 mutant cells at a 10nM concentration, as this dose has previously been reported to normalize the altered signaling responses associated with FHH2-causing $G\alpha_{11}$ mutations *in vitro* (23). An assessment of Ca^{2+}_i responses showed 10nM cinacalcet to induce a leftward shift of the concentration-response curve of cells expressing the Gly195 mutant $G\alpha_{11}$ protein (Figure 2C) and decrease their mean EC_{50} value to 2.70mM (95% CI, 2.60–2.80 mM), a value that was indistinguishable from the EC_{50} of untreated WT cells (Figure 2C and D). Thus, cinacalcet normalised the signaling responses of Gly195 mutant cells.

In vivo functional analysis in mice harboring the germline Gna11 Asp195Gly mutation. To investigate the *in vivo* effects of the Asp195Gly $G\alpha_{11}$ mutation on Ca^{2+}_o homeostasis, ENU mutagenesis-derived mice harboring this mutation were established on the C3H inbred genetic background (24). DNA sequence analysis confirmed the mutant mice to harbor a germline A-to-G transition at c.584A>G at codon 195 of the $G\alpha_{11}$ protein resulting in an Asp (D) to Gly (G) missense substitution (Figure 3A and B). This mutation led to a gain of a *HaeIII* restriction endonuclease site (Figure 3C), which was used to confirm the presence of the mutation (Figure 3D), and for genotyping of subsequent generations of mice. Heterozygous-affected (*Gna11*$^{+/195G}$) mice were healthy and fertile, and an analysis of offspring bred from crosses of *Gna11*$^{+/195G}$ mice yielded homozygous-affected (*Gna11*$^{195G/195G}$) mice and significant deviations from the Mendelian inheritance expected ratio of 1:2:1 for the WT (*Gna11*$^{+/+}$): *Gna11*$^{+/195G}$ and *Gna11*$^{195G/195G}$ genotypes were not observed among the weaned mice, thereby indicating that the homozygous *Gna11*$^{195G/195G}$ mice were viable and did not have embryonic or neonatal lethality (Table 1). Moreover, *Gna11*$^{195G/195G}$ mice had a normal body weight compared to WT (*Gna11*$^{+/+}$) and *Gna11*$^{+/195G}$ littermates (Table 2). Thus, *Gna11*$^{195G/195G}$ mice did not have evidence of growth retardation or neonatal lethality to suggest an NSHPT phenotype. However, plasma biochemical analysis revealed *Gna11*$^{+/195G}$ and *Gna11*$^{195G/195G}$ mice to be significantly hypercalcemic compared to *Gna11*$^{+/+}$ mice (Figure 4A). Moreover, *Gna11*$^{195G/195G}$ mice had significantly reduced plasma phosphate concentrations and raised plasma PTH concentrations when compared to *Gna11*$^{+/+}$ mice, whereas *Gna11*$^{+/195G}$ mice had plasma phosphate and PTH

concentrations that were similar to those of *Gna11*$^{+/+}$ mice (Figure 4B and C). Furthermore, the fractional excretion of calcium was not altered in *Gna11*$^{+/195G}$ or *Gna11*$^{195G/195G}$ mice compared to *Gna11*$^{+/+}$ mice (Figure 4D and Table 3). However, there were gender differences in these calcitropic phenotypes, as follows. Thus, female *Gna11*$^{195G/195G}$ mice were significantly more hypercalcemic than male *Gna11*$^{195G/195G}$ mice and female *Gna11*$^{+/195G}$ mice (Table 2). In addition, female *Gna11*$^{195G/195G}$ mice, but not the *Gna11* mutant males, had significant hypophosphatemia with a significant reduction in the tubular maximum reabsorption of phosphate (Table 3), and a raised alkaline phosphatase activity compared to female *Gna11*$^{+/+}$ mice (Table 2, Supplementary Figure 2). Significant differences were not observed in plasma electrolytes, urea and creatinine concentrations, or in 1,25-dihydroxyvitamin D or fibroblast growth factor-23 (FGF-23) concentrations in male or female *Gna11*$^{+/195G}$ and *Gna11*$^{195G/195G}$ mice, when compared to respective *Gna11*$^{+/+}$ mice (Table 2). The fractional excretions of sodium and potassium were also not different between male and female mutant mice and respective *Gna11*$^{+/+}$ mice (Table 3). Finally, whole body dual-energy X-ray absorptiometry (DXA) did not reveal significant differences in the bone mineral content or bone mineral density (BMD) between male and female mutant mice and respective *Gna11*$^{+/+}$ mice (Table 4).

To determine whether the hypercalcemia of *Gna11*$^{+/195G}$ and *Gna11*$^{195G/195G}$ mice may be improved by *in vivo* calcimimetic treatment we administered cinacalcet to WT and mutant mice. A pilot dose-ranging study in WT mice showed that a single oral gavage 30 mg/kg dose of cinacalcet significantly lowered plasma PTH concentrations, when compared to vehicle-treated mice (Supplementary Figure 3). This dose (30mg/kg) of cinacalcet was therefore administered by oral gavage to *Gna11*$^{+/+}$, *Gna11*$^{+/195G}$ and *Gna11*$^{195G/195G}$ mice, and plasma samples were then taken at 0, 1, 2, 4, 6 and 24h post-dose for the measurement of PTH, calcium, phosphate, urea, creatinine and albumin concentrations. Administration of cinacalcet significantly: decreased plasma PTH concentrations in *Gna11*$^{+/+}$, *Gna11*$^{+/195G}$ and *Gna11*$^{195G/195G}$ mice by ≥60% at 1h post-dose, with values returning to baseline by 4-6h post-dose (Figure 5A-C); and reduced plasma albumin-adjusted calcium concentrations in *Gna11*$^{+/+}$, *Gna11*$^{+/195G}$ and *Gna11*$^{195G/195G}$ mice between 2-6h post-dose, with values returning to baseline by 24h post-dose (Figure 5D-F). Cinacalcet treatment also resulted

in a transient rise in plasma phosphate concentrations in *Gna11*$^{+/+}$, *Gna11*$^{+/195G}$ and *Gna11*$^{195G/195G}$ mice (Figure 5G-I), but was not associated with any increases in plasma concentrations of urea or creatinine (Supplementary Figure 4). Thus, these studies demonstrated that cinacalcet is effective *in vivo* and can reduce raised plasma calcium and PTH concentrations observed in *Gna11* mutant mice with a loss-of-function $G\alpha_{11}$ mutation, that is representative of FHH2.

Discussion

We have established a mouse model for FHH2 and this will enable the calcitropic roles of $G\alpha_{11}$ to be further evaluated, and also facilitate further pathophysiological studies, that are difficult to pursue in the few reported patients with this condition. Our results revealed that heterozygous-affected (*Gna11*$^{+/195G}$) mice had a similar plasma biochemical phenotype to that reported for FHH2 patients, who also harbour heterozygous loss-of-function $G\alpha_{11}$ mutations (Table 5) (3, 10). Thus, *Gna11*$^{+/195G}$ mice had mild hypercalcemia in association with normal plasma PTH concentrations, and also had no alterations in the plasma concentrations of phosphate and creatinine, or in alkaline phosphatase activity, which is consistent with the reported phenotype of FHH2 patients (Table 5) (3, 10). *Gna11*$^{+/195G}$ mice additionally had normal plasma magnesium concentrations, which is consistent with one reported FHH2 proband (3), but which contrasts with the hypermagnesemia reported in a multi-generational FHH2 kindred (3). A key finding of this study is that *Gna11*$^{+/195G}$ and *Gna11*$^{195G/195G}$ mice had no alterations in urinary calcium excretion and this would be consistent with studies of FHH2 patients, which have reported that not all FHH2 patients have a low fractional excretion of calcium (Table 5) (3, 10). The absence of a urinary calcium phenotype in *Gna11*$^{+/195G}$ and *Gna11*$^{195G/195G}$ mice is also consistent with the reported findings in mice and humans harboring germline gain-of-function $G\alpha_{11}$ mutations that is associated with hypocalcemia and reduced plasma PTH concentations, but with mild or no alterations in urinary calcium excretion (25-27). These studies highlight a potential difference in the calcitropic phenotype of disorders caused by germline $G\alpha_{11}$ mutations and that of disorders caused by germline CaSR mutations, and suggest that the $G\alpha_{11}$ protein may not play a major role in the renal handling of calcium. Thus, it remains to be established whether hypocalciuria represents a major component of the FHH2 disorder in humans. Furthermore, DXA analysis did not reveal any alterations in the BMD values of *Gna11*$^{195G/195G}$ mice, which also suggests that the $G\alpha_{11}$ protein may not influence bone mass.

Our studies of homozygous-affected (*Gna11*$^{195G/195G}$) mice have highlighted the importance of $G\alpha_{11}$ for parathyroid gland function and PTH secretion, as *Gna11*$^{195G/195G}$ mice had more pronounced hypercalcemia, hypophosphatemia, and significantly raised plasma PTH concentrations, consistent

with primary hyperparathyroidism (28). Moreover, female *Gna11*$^{195G/195G}$ mice also had significant elevations of plasma alkaline phosphatase activity, which is consistent with an elevated bone turnover associated with this likely primary hyperparathyroidism. However, the hypercalcemic phenotype of *Gna11*$^{195G/195G}$ mice was in general milder than that observed in humans or mice harboring biallelic loss-of-function CaSR mutations, which typically lead to the life-threatening disorder of NSHPT (12, 24). A possible explanation for the milder hypercalcemic phenotype observed in the *Gna11*$^{195G/195G}$ mice is that the loss of $G\alpha_{11}$ function caused by the Asp195Gly mutation *in vivo* was partially compensated by the WT $G\alpha_q$ protein, which in the parathyroid glands continued to mediated signal transduction by the CaSR. Indeed, the importance of the $G\alpha_{11}$ and $G\alpha_q$ proteins for parathyroid gland function has been demonstrated by studies of mice with a parathyroid-specific ablation of both $G\alpha_{11}$ and $G\alpha_q$, which have been reported to develop features of NSHPT such as severe hypercalcemia, skeletal demineralisation, growth retardation and early postnatal death (7). The hypercalcemia observed in *Gna11*$^{195G/195G}$ mice was more severe in females compared to males, and such gender differences have not previously been reported in studies of FHH patients. However, gender differences have been noted in primary hyperparathyroidism patients, with females being more commonly affected than males (29). Moreover, estrogen may play a role in the pathogenesis and severity of primary hyperparathyroidism, as highlighted by a study that showed the potential involvement of estrogen signaling in parathyroid function and disease (30), and such effects may have contributed to the more severe hypercalcemia of female *Gna11*$^{195G/195G}$ mice.

There is currently no effective treatment for FHH2, and we therefore evaluated the therapeutic potential of cinacalcet, which is a licenced CaSR positive allosteric modulator (13), for this condition. *In vitro* studies have previously reported that nanomolar concentrations of cinacalcet can successfully rectify the altered signalling responses of HEK-CaSR cells expressing FHH2-associated $G\alpha_{11}$ mutant proteins (23). Consistent with these findings, our study showed a 10 nM concentration of cinacalcet to normalise the Ca^{2+}_i responses of HEK-CaSR cells expressing the mutant Gly195 $G\alpha_{11}$ protein. Moreover, oral administration of a single 30 mg/kg cinacalcet dose led to a transient suppression of PTH secretion in *Gna11*$^{+/195G}$ and *Gna11*$^{195G/195G}$ mice, and this was associated with a sustained reduction in plasma calcium concentrations, which lasted for ≥ 6h. This

dose of cinacalcet was well tolerated in the mice, and did not lead to hypocalcemia, with mean plasma calcium concentrations remaining at >2.0 mmol/L. However, transient hyperphosphatemia was noted in cinacalcet-treated mice, which was likely to be a consequence of suppressed PTH secretion (31). These results suggest that calcimimetics such as cinacalcet will likely be of benefit for FHH2 patients, who also harbor loss-of-function $G\alpha_{11}$ mutations (23).

In summary, we have established a mouse model for FHH2 and have shown the *in vivo* efficacy of cinacalcet in reducing plasma calcium and PTH concentrations, thereby illustrating the potential utility of this CaSR allosteric modulator for the treatment of hypercalcemia in patients with FHH2.

Methods

Animals. ENU-treated G0 C57BL/6J male mice were mated to C3H/HeH (C3H) mice to produce G1 progeny and tissue-DNA samples from >10,000 G1 ENU mutagenized male mice, together with their sperm, was archived, as reported (14). These tissue-DNA samples were used to identify *Gna11* variants, by melt curve analysis of PCR products utilizing a Lightscanner and gene-specific primers (BioFire Diagnostics, Inc., Salt Lake City, Utah, USA), and sperm from mice with *Gna11* variants was used for IVF to generate G2 progeny on a C3H background strain, as reported (16, 24). Heterozygous-affected (*Gna11*$^{+/I95G}$) mutant male and female mice were intercrossed to generate homozygous (*Gna11*$^{I95G/I95G}$) mice, which were studied along with their *Gna11*$^{+/I95G}$ and WT (*Gna11*$^{+/+}$) littermates. All study mice were housed in a controlled environment at the MRC Harwell Institute in accordance with UK Home Office and MRC Welfare guidance. Mice were fed on a standard diet (Rat and Mouse number 3, Special Diet Services, UK) that contained 1.15% calcium, 0.58% phosphate and 4089 IU/kg of vitamin D, and provided with water *ad libitum* (25, 32).

Compounds. Cinacalcet (AMG-073 HCL) was obtained from Cambridge Bioscience (catalog no. CAY16042) and dissolved in a 20% aqueous solution of 2-hydroxypropyl-β-cyclodextrin (Sigma-Aldrich, catalog no. H107) prior to use in *in vitro* and *in vivo* studies.

DNA sequence analysis. Genomic DNA was isolated from auricular biopsies using DNA extraction buffer (10mM NaCl, 20mM Tris-HCl, pH8.0, 1mM EDTA, 10% sodium dodecyl sulfate (SDS)) and Proteinase K solution (ThermoFisher, Carlsbad, USA) (25). Genomic DNA was used with *Gna11* gene-specific primers (SigmaAldrich, Gillingham, UK) to perform PCR amplification, followed by dideoxynucleotide sequencing using the BigDye Terminator v3.1 Cycle Sequencing Kit, and an automated detection system (ABI 3730 Automated capillary sequencer, ThermoFisher), as reported (25). MutationTasting (http://www.mutationtaster.org/) and Polyphen-2 software was used to predict variant pathogenicity (33, 34). The *Gna11* germline mutation was confirmed by *HaeIII* restriction endonuclease analysis (New England Biolabs), as previously described (3, 4).

Protein sequence alignment and three-dimensional modeling. Protein sequences of $G\alpha_{11}$ orthologs and paralogs were aligned with ClustalOmega (35). The PyMOL Molecular Graphics System (Version 1.2r3pre, Schrödinger, LLC) was used for structural modeling based on the complexed crystal structure of $G\alpha_q$, which has 90% identity with $G\alpha_{11}$ at the amino acid level (Protein Data Bank, accession no. 4GNK) (18). The effect of the $G\alpha_{11}$ mutations upon $G\alpha_{11}$ structure was modeled using the PyMod plug-in and Modeller (36).

Cell Culture and Transfection. Functional studies were undertaken using a human *GNA11* construct (3), as the human and mouse $G\alpha_{11}$ proteins share an overall amino acid identity of 98% (25), and are 100% identical in the region surrounding the mutated site. The Gly195 mutation was introduced by site-directed mutagenesis (QuikChange Lightning, Agilent Technologies) into a pBI-CMV2-*GNA11-GFP* expression construct, as reported (3); and WT and mutant pBI-CMV2-*GNA11-GFP* constructs were transiently transfected into HEK293 cells stably expressing the full-length human *CASR* cDNA (HEK-CaSR), as described (3). HEK-CaSR cells were maintained in Dulbecco's Modified Eagle Medium (DMEM)-Glutamax media (ThermoFisher) with 10% fetal bovine serum (Gibco) and 400µg/mL geneticin (ThermoFisher) at 37ºC, 5% CO_2 (3). Successful transfection was confirmed by visualising GFP fluorescence using an Eclipse E400 fluorescence microscope with an epifluorescence filter, and images were captured using a DXM1200C digital camera and NIS Elements software (Nikon) (3, 11). The expression of $G\alpha_{11}$, CaSR, GFP, calnexin and GAPDH proteins was confirmed by Western blot analyses using anti-$G\alpha_{11}$ (D-6, sc-390382, Santa Cruz Biotechnologies), anti-CaSR (5C10, ADD, ab19347, Abcam), anti-GFP (B-2, sc-9996, Santa Cruz Biotechnologies), anti-calnexin (AB2301, Millipore), and anti-GAPDH (AM4300, Ambion) antibodies, respectively. The Western blots were visualised using an Immuno-Star Western C kit (BioRad) on a BioRad Chemidoc XRS+ system (3, 10).

Measurement of Ca^{2+}_i responses. The Ca^{2+}_i responses of HEK293-CaSR cells expressing WT or mutant $G\alpha_{11}$ proteins were measured by Fluo-4 calcium assays adapted from methods previously

published (22). HEK-CaSR cells were plated in poly-L-lysine treated black-walled 96-well plates (Corning), and transiently transfected with 1000µg/ml pBI-CMV2-*GNA11-GFP*. On the following day, cells were incubated in serum-free media for 2h, then loaded with the Fluo-4 Ca^{2+}-binding dye, prepared according to manufacturer's instructions (Invitrogen). Cells were loaded for 40 minutes at 37°C, then either a 20% aqueous solution of 2-hydoxypropyl-β-cyclodextrin (vehicle), or 10nM cinacalcet was added, and cells incubated for a further 20 minutes at 37°C (19). Baseline measurements were made and increasing doses of $CaCl_2$ injected into each well, using an automated system. Changes in Ca^{2+}_i were recorded on a PHERAstar instrument (BMG Labtech) at 37°C with an excitation filter of 485nm and an emission filter of 520nm. The peak mean fluorescence ratio of the transient response after each individual stimulus was measured using MARS data analysis software (BMG Labtech), and expressed as a normalized response. Nonlinear regression of concentration-response curves was performed with GraphPad Prism using the normalized response at each $[Ca^{2+}]_o$ for each separate experiment for the determination of the EC_{50} (i.e. $[Ca^{2+}]_o$ required for 50% of the maximal response).

Metabolic cage studies and biochemical analysis. Thirteen to 15 week old mice were individually housed in metabolic cages (Techniplast) for 24h with free access to food and water. Mice were allowed to acclimatise to their environment over a 72h period, as described (37), prior to collection of 24h urine samples. Twenty-four hour urine samples were collected in tubes containing sodium azide, and blood samples collected from the lateral tail vein under topical local anesthesia (38) or from the retro-orbital vein into lithium heparin Microvette tubes (Sarstedt) following terminal isoflurane anaesthesia, as described (25, 32). Plasma and urine were analyzed for sodium, potassium, total calcium, phosphate, magnesium, urea, creatinine, and alkaline phosphatase activity on a Beckman Coulter AU680 analyzer (25, 32). Plasma calcium was adjusted for variations in albumin concentrations using the formula: (plasma calcium (mmol/L) – [(plasma albumin – mean albumin (g/L) of respective male and female WT mice) x 0.02], as reported (39). Hormones were measured as follows: PTH using a two-site ELISA specific for mouse intact PTH (Immutopics, San Clemente, USA); 1,25-dihydroxyvitamin D by a two-step process involving purification by immunoextraction

and quantification by enzyme immunoassay (Immunodiagnostic Systems); and FGF-23 using a two-site ELISA kit (Kainos Laboratories), as described (25, 39). The fractional excretion of sodium, potassium, and calcium were calculated using the formula $U_x/P_x*P_{Cr}/U_{Cr}$, where U_x is the urinary concentration of the filtered substance (substance *x*) in mmol/L, P_x is the plasma concentration of substance *x* in mmol/L, U_{Cr} is the urinary concentration of creatinine in mmol/L, and P_{Cr} is the plasma concentration of creatinine in mmol/L. The ratio of tubular maximum reabsorption of phosphate to GFR (TmP/GFR) was calculated using the following formula: $P_{Pi}*(1-(U_{Pi}/P_{Pi}*P_{Cr}/U_{Cr}))$, where P_{Pi} is the plasma concentration of phosphate and U_{Pi} is the urine concentration of phosphate (25, 32).

Skeletal imaging. Bone mineral content and density were assessed by whole body DXA scanning, which was performed on mice anesthetized by inhaled isoflurane and using a Lunar Piximus densitometer (GE Medical Systems), as reported (25). DXA images were analyzed using Piximus software, as reported (25).

Statistical analysis. All *in vitro* studies involved eight biological replicates. Statistical comparisons of the Ca^{2+}_i EC_{50} responses, were undertaken using the *F*-test, as reported (3). For the *in vivo* studies, a Kruskal-Wallis test was undertaken for multiple comparisons, and any significant differences identified were further assessed using the Dunn's test for non-parametric pairwise multiple comparisons (25). All analyses were performed using GraphPad Prism (GraphPad), and a value of $p<0.05$ was considered significant for all analyses.

Study approval. Animal studies were approved by the MRC Harwell Institute Ethical Review Committee and were licensed under the Animal (Scientific Procedures) Act 1986, issued by the UK Government Home Office Department (PPL30/2433 and PPL30/3271).

Author Contributions

Designing research studies (S.A.H., F.M.H., C.M.G., M.A.N., S.D.M.B., R.D.C., R.V.T.), conducting experiments (S.A.H., C.M.G., A.P., M.S., T.A.H., S.W.), acquiring and analysing data (S.A.H., F.M.H., C.M.G., S.E.P.), wrote the manuscript (S.A.H., F.M.H., C.M.G., R.V.T.).

Acknowledgements

This work was supported by the United Kingdom Medical Research Council (MRC) programme grants - G9825289 and G1000467 (to M.A.N., F.M.H., C.M.G. and R.V.T). S.A.H. was a Wellcome Trust Clinical Training Fellow; and R.V.T. is a Wellcome Trust Investigator and NIHR Senior Investigator. We thank R. Head for technical assistance.

References

1. Hannan FM, Babinsky VN, and Thakker RV. Disorders of the calcium-sensing receptor and partner proteins: insights into the molecular basis of calcium homeostasis. *J Mol Endocrinol.* 2016;57(3):R127-42.
2. Hannan FM, Nesbit MA, Zhang C, Cranston T, Curley AJ, Harding B, Fratter C, Rust N, Christie PT, Turner JJ, et al. Identification of 70 calcium-sensing receptor mutations in hyper- and hypo-calcaemic patients: evidence for clustering of extracellular domain mutations at calcium-binding sites. *Hum Mol Genet.* 2012;21(12):2768-78.
3. Nesbit MA, Hannan FM, Howles SA, Babinsky VN, Head RA, Cranston T, Rust N, Hobbs MR, Heath H, 3rd, and Thakker RV. Mutations affecting G-protein subunit alpha11 in hypercalcemia and hypocalcemia. *N Engl J Med.* 2013;368(26):2476-86.
4. Nesbit MA, Hannan FM, Howles SA, Reed AA, Cranston T, Thakker CE, Gregory L, Rimmer AJ, Rust N, Graham U, et al. Mutations in AP2S1 cause familial hypocalciuric hypercalcemia type 3. *Nat Genet.* 2013;45(1):93-7.
5. Hofer AM, and Brown EM. Extracellular calcium sensing and signalling. *Nat Rev Mol Cell Biol.* 2003;4(7):530-8.
6. Conigrave AD, and Ward DT. Calcium-sensing receptor (CaSR): pharmacological properties and signaling pathways. *Best practice & research Clinical endocrinology & metabolism.* 2013;27(3):315-31.
7. Wettschureck N, Lee E, Libutti SK, Offermanns S, Robey PG, and Spiegel AM. Parathyroid-specific double knockout of Gq and G11 alpha-subunits leads to a phenotype resembling germline knockout of the extracellular Ca2+ -sensing receptor. *Mol Endocrinol.* 2007;21(1):274-80.
8. Dare E, Kifor O, Brown EM, and Weber G. Characterization of the phosphatidylinositol-specific phospholipase C isozymes present in the bovine parathyroid and in human kidney HEK293 cells stably transfected with the human parathyroid Ca2+-sensing receptor. *J Mol Endocrinol.* 1998;21(1):7-17.
9. Corbetta S, Lania A, Filopanti M, Vicentini L, Ballare E, and Spada A. Mitogen-activated protein kinase cascade in human normal and tumoral parathyroid cells. *J Clin Endocrinol Metab.* 2002;87(5):2201-5.
10. Gorvin CM, Cranston T, Hannan FM, Rust N, Qureshi A, Nesbit MA, and Thakker RV. G-Protein Subunit-alpha11 Loss-of-Function Mutation, Thr54Met, Causing Familial Hypocalciuric Hypercalcemia Type 2 (FHH2). *J Bone Miner Res.* 2016;31(1200-6.
11. Hannan FM, Howles SA, Rogers A, Cranston T, Gorvin CM, Babinsky VN, Reed AA, Thakker CE, Bockenhauer D, Brown RS, et al. Adaptor protein-2 sigma subunit mutations causing familial hypocalciuric hypercalcaemia type 3 (FHH3) demonstrate genotype-phenotype correlations, codon bias and dominant-negative effects. *Hum Mol Genet.* 2015;24(18):5079-92.
12. Ho C, Conner DA, Pollak MR, Ladd DJ, Kifor O, Warren HB, Brown EM, Seidman JG, and Seidman CE. A mouse model of human familial hypocalciuric hypercalcemia and neonatal severe hyperparathyroidism. *Nat Genet.* 1995;11(4):389-94.
13. Nemeth EF, and Goodman WG. Calcimimetic and Calcilytic Drugs: Feats, Flops, and Futures. *Calcif Tissue Int.* 2016;98(4):341-58.
14. Acevedo-Arozena A, Wells S, Potter P, Kelly M, Cox RD, and Brown SD. ENU mutagenesis, a way forward to understand gene function. *Annu Rev Genomics Hum Genet.* 2008;9(49-69.
15. Piret SE, and Thakker RV. Mouse models for inherited endocrine and metabolic disorders. *J Endocrinol.* 2011;211(3):211-30.
16. Gorvin CM, Rogers A, Stewart M, Paudyal A, Hough TA, Teboul L, Wells S, Brown SDM, Cox RD, and Thakker RV. N-ethyl-N-nitrosourea–Induced Adaptor Protein 2 Sigma Subunit 1 (*Ap2s1*) Mutations Establish Ap2s1 Loss-of-Function Mice. *JBMR Plus.* 2017. DOI: 10.1002/jbm4.10001 (*In press*).
17. Oldham WM, and Hamm HE. Heterotrimeric G protein activation by G-protein-coupled receptors. *Nat Rev Mol Cell Biol.* 2008;9(1):60-71.

18. Lyon AM, Dutta S, Boguth CA, Skiniotis G, and Tesmer JJ. Full-length Galpha(q)-phospholipase C-beta3 structure reveals interfaces of the C-terminal coiled-coil domain. *Nat Struct Mol Biol.* 2013;20(3):355-62.
19. Tesmer VM, Kawano T, Shankaranarayanan A, Kozasa T, and Tesmer JJ. Snapshot of activated G proteins at the membrane: the Galphaq-GRK2-Gbetagamma complex. *Science.* 2005;310(5754):1686-90.
20. Waldo GL, Ricks TK, Hicks SN, Cheever ML, Kawano T, Tsuboi K, Wang X, Montell C, Kozasa T, Sondek J, et al. Kinetic scaffolding mediated by a phospholipase C-beta and Gq signaling complex. *Science.* 2010;330(6006):974-80.
21. Flock T, Hauser AS, Lund N, Gloriam DE, Balaji S, and Babu MM. Selectivity determinants of GPCR-G-protein binding. *Nature.* 2017;545(7654):317-22.
22. Leach K, Gregory KJ, Kufareva I, Khajehali E, Cook AE, Abagyan R, Conigrave AD, Sexton PM, and Christopoulos A. Towards a structural understanding of allosteric drugs at the human calcium-sensing receptor. *Cell Res.* 2016;26(5):574-92.
23. Babinsky VN, Hannan FM, Gorvin CM, Howles SA, Nesbit MA, Rust N, Hanyaloglu AC, Hu J, Spiegel AM, and Thakker RV. Allosteric Modulation of the Calcium-Sensing Receptor Rectifies Signaling Abnormalities Associated with G-protein alpha-11 Mutations causing Hypercalcemic and Hypocalcemic Disorders. *J Biol Chem.* 2016;291(10876-85.
24. Loh NY, Bentley L, Dimke H, Verkaart S, Tammaro P, Gorvin CM, Stechman MJ, Ahmad BN, Hannan FM, Piret SE, et al. Autosomal dominant hypercalciuria in a mouse model due to a mutation of the epithelial calcium channel, TRPV5. *PLoS One.* 2013;8(1):e55412.
25. Gorvin CM, Hannan FM, Howles SA, Babinsky VN, Piret SE, Rogers A, Freidin AJ, Stewart M, Paudyal A, Hough TA, et al. Gα11 mutation in mice causes hypocalcemia rectifiable by calcilytic therapy. *JCI Insight.* 2017;2(e91103.
26. Li D, Opas EE, Tuluc F, Metzger DL, Hou C, Hakonarson H, and Levine MA. Autosomal dominant hypoparathyroidism caused by germline mutation in GNA11: phenotypic and molecular characterization. *J Clin Endocrinol Metab.* 2014;99(9):E1774-83.
27. Roszko KL, Bi R, Gorvin CM, Brauner-Osborne H, Xiong XF, Inoue A, Thakker RV, Stromgaard K, Gardella T, and Mannstadt M. Knockin mouse with mutant Galpha11 mimics human inherited hypocalcemia and is rescued by pharmacologic inhibitors. *JCI Insight.* 2017;2(3):e91079.
28. Fraser WD. Hyperparathyroidism. *Lancet.* 2009;374(9684):145-58.
29. Adami S, Marcocci C, and Gatti D. Epidemiology of primary hyperparathyroidism in Europe. *J Bone Miner Res.* 2002;17 Suppl 2(N18-23.
30. Haglund F, Ma R, Huss M, Sulaiman L, Lu M, Nilsson IL, Hoog A, Juhlin CC, Hartman J, and Larsson C. Evidence of a functional estrogen receptor in parathyroid adenomas. *J Clin Endocrinol Metab.* 2012;97(12):4631-9.
31. Howles SA, Hannan FM, Babinsky VN, Rogers A, Gorvin CM, Rust N, Nesbit MA, Thakker RV, Richardson T, and McKenna MJ. Cinacalcet for Symptomatic Hypercalcemia Caused by AP2S1 Mutations. *N Engl J Med.* 2016;374(14):1396-8.
32. Hannan FM, Walls GV, Babinsky VN, Nesbit MA, Kallay E, Hough TA, Fraser WD, Cox RD, Hu J, Spiegel AM, et al. The Calcilytic Agent NPS 2143 Rectifies Hypocalcemia in a Mouse Model With an Activating Calcium-Sensing Receptor (CaSR) Mutation: Relevance to Autosomal Dominant Hypocalcemia Type 1 (ADH1). *Endocrinology.* 2015;156(9):3114-21.
33. Adzhubei IA, Schmidt S, Peshkin L, Ramensky VE, Gerasimova A, Bork P, Kondrashov AS, and Sunyaev SR. A method and server for predicting damaging missense mutations. *Nat Methods.* 2010;7(4):248-9.
34. Schwarz JM, Cooper DN, Schuelke M, and Seelow D. MutationTaster2: mutation prediction for the deep-sequencing age. *Nat Methods.* 2014;11(4):361-2.
35. Sievers F, Wilm A, Dineen D, Gibson TJ, Karplus K, Li W, Lopez R, McWilliam H, Remmert M, Soding J, et al. Fast, scalable generation of high-quality protein multiple sequence alignments using Clustal Omega. *Mol Syst Biol.* 2011;7(539.
36. Bramucci E, Paiardini A, Bossa F, and Pascarella S. PyMod: sequence similarity searches, multiple sequence-structure alignments, and homology modeling within PyMOL. *BMC Bioinformatics.* 2012;13 Suppl 4(S2.

37. Stechman MJ, Ahmad BN, Loh NY, Reed AA, Stewart M, Wells S, Hough T, Bentley L, Cox RD, Brown SD, et al. Establishing normal plasma and 24-hour urinary biochemistry ranges in C3H, BALB/c and C57BL/6J mice following acclimatization in metabolic cages. *Lab Anim.* 2010;44(3):218-25.
38. Bentley L, Esapa CT, Nesbit MA, Head RA, Evans H, Lath D, Scudamore CL, Hough TA, Podrini C, Hannan FM, et al. An N-ethyl-N-nitrosourea induced corticotropin-releasing hormone promoter mutation provides a mouse model for endogenous glucocorticoid excess. *Endocrinology.* 2014;155(3):908-22.
39. Esapa CT, Hannan FM, Babinsky VN, Potter P, Thomas GP, Croucher PI, Brown MA, Brown SD, Cox RD, and Thakker RV. N-ethyl-N-Nitrosourea (ENU) induced mutations within the klotho gene lead to ectopic calcification and reduced lifespan in mouse models. *PLoS One.* 2015;10(4):e0122650.
40. Hsieh KP, and Martin TF. Thyrotropin-releasing hormone and gonadotropin-releasing hormone receptors activate phospholipase C by coupling to the guanosine triphosphate-binding proteins Gq and G11. *Mol Endocrinol.* 1992;6(10):1673-81.
41. Heath H, 3rd, Leppert MF, Lifton RP, and Penniston JT. Genetic linkage analysis in familial benign hypercalcemia using a candidate gene strategy. I. Studies in four families. *J Clin Endocrinol Metab.* 1992;75(3):846-51.

Table 1. Proportion of offspring bred from crosses of *Gna11*$^{+/195G}$ x *Gna11*$^{+/195G}$ mice

Genotype	**Expected number of offspring (n=358 born)**	**Observed number of offspring (n=234 weaned)**
+/+	89 (25%)	56 (24%)
+/195G	180 (50%)	127 (54%)
195G /195G	89 (25%)	51 (22%)

The Mendelian inheritance expected ratio from heterozygous crosses is 1:2:1, and chi-square analysis shows no significant differences in the expected *vs.* observed ratios of offspring genotypes at weaning (i.e. 19-21 days of age) ($x^2 = 1.0$, *degrees of freedom = 2*).

Table 2. Age, weight and plasma biochemical profile of *Gna11*$^{+/+}$, *Gna11*$^{+/195G}$ and *Gna11*$^{195G/195G}$ mice

Parameter	Male			Female		
	Gna11$^{+/+}$	*Gna11*$^{+/195G}$	*Gna11*$^{195G/195G}$	*Gna11*$^{+/+}$	*Gna11*$^{+/195G}$	*Gna11*$^{195G/195G}$
Age (weeks)	13.9±0.1 (n=12)	14.0±0.1 (n=13)	13.9±0.1 (n=14)	13.8±0.1 (n=10)	13.8±0.1 (n=15)	13.6±0.1 (n=13)
Weight (g)	31.7±0.7 (n=12)	31.4±1.1 (n=13)	32.3±0.9 (n=14)	27.5±0.8 (n=13)	30.2±0.9 (n=15)	30.2±0.6 (n=13)
Sodium (mmol/L)	149±0.7 (n=12)	151±0.5 (n=13)	150±0.6 (n=13)	149±0.6 (n=10)	148±0.7 (n=15)	147±0.6 (n=13)
Potassium (mmol/L)	5.4±0.1 (n=12)	5.2±0.1 (n=13)	5.3±0.1 (n=13)	5.0±0.1 (n=10)	4.9±0.1 (n=15)	4.9±0.2 (n=13)
Urea (mmol/L)	10.7±0.6 (n=12)	9.8±0.3 (n=13)	10.1±0.4 (n=13)	8.6±0.6 (n=10)	8.8±0.2 (n=15)	9.0±0.3 (n=12)
Creatinine (µmol/L)	11.6±0.6 (n=12)	10.8±0.7 (n=13)	12.0±0.7 (n=13)	12.7±0.4 (n=10)	12.8±0.4 (n=15)	12.4±0.4 (n=13)
Calcium (mmol/L)	2.36±0.02 (n=12)	2.40±0.02 (n=12)	2.48±0.02 (n=13)***	2.40+0.03 (n=10)	2.46±0.01 (n=15)	2.59±0.02 (n=13)***$^{\$}$
Adj-calcium (mmol/L)[A]	2.36±0.02 (n=12)	2.41±0.02 (n=12)	2.48±0.02 (n=13)***	2.39±0.02 (n=10)	2.45±0.01 (n=15)	2.58±0.02 (n=13)***$^{\$}$
Albumin (g/L)	25.2±0.3 (n=12)	24.8±0.3 (n=12)	25.0±0.2 (n=13)	26.2±0.4 (n=10)	26.5±0.4 (n=15)	26.9±0.4 (n=13)
Magnesium (mmol/L)	0.80±0.02 (n=12)	0.76±0.02 (n=13)	0.76±0.02 (n=13)	0.81±0.02 (n=10)	0.83±0.02 (n=15)	0.85±0.02 (n=13)
Phosphate (mmol/L)	1.67±0.11 (n=12)	1.65±0.08 (n=13)	1.51±0.08 (n=13)	2.04±0.12 (n=10)	1.73±0.05 (n=15)	1.66±0.11 (n=13)*
ALP (U/L)	93.2±3.3 (n=12)	90.8±4.9 (n=13)	98.5±3.2 (n=13)	120±4.5 (n=10)	132±3.5 (n=15)	142±6.5 (n=13)*
PTH (ng/L)	417±37 (n=8)	562±54 (n=12)	813±63 (n=13)***	290±34 (n=10)	405±43 (n=12)	535±36 (n=9)**
1,25D (pmol/L)	74.5±11 (n=12)	64.7±10 (n=10)	90.7±19 (n=12)	72.8±9 (n=10)	76.8±6 (n=14)	86.3±7 (n=13)
FGF-23 (ng/L)	149±7 (n=12)	170±5 (n=11)	173±8 (n=12)	150±4 (n=10)	146±7 (n=14)	160±8 (n=13)

[A]Plasma calcium concentrations were adjusted according to the mean plasma albumin concentration of respective male and female WT mice. Adj-calcium, albumin-adjusted calcium; ALP, alkaline phosphatase activity; PTH, parathyroid hormone; 1,25D, 1,25 dihydroxyvitamin D; FGF-23, fibroblast growth factor-23. All values are expressed as mean ± SEM. A Kruskal-Wallis test followed by Dunn's test for non-parametric pairwise multiple comparisons were used to compare mutant mice with WT mice, and a Mann-Whitney U test was used to compare respective male and female mice. *p<0.05, **p<0.01, ***p<0.001 compared to respective *Gna11*$^{+/+}$ mice. $^{\$}$p<0.001 compared to respective male mice.

Table 3. Urine biochemical profile of *Gna11*$^{+/+}$, *Gna11*$^{+/195G}$ and *Gna11*$^{195G/195G}$ mice

Parameter	Male			Female		
	Gna11$^{+/+}$	*Gna11*$^{+/195G}$	*Gna11*$^{195G/195G}$	*Gna11*$^{+/+}$	*Gna11*$^{+/195G}$	*Gna11*$^{195G/195G}$
24hr Ca	4.9±0.4 (n=9)	5.9±0.5 (n=13)	6.4±0.7 (n=13)	11.7±1.3 (n=10)$^{\$\$}$	16.3±2.4 (n=15)$^{\$\$}$	17.0±1.7 (n=12)$^{\$\$}$
Ca/Cr	0.30±0.02 (n=9)	0.31±0.02 (n=12)	0.32±0.02 (n=13)	0.57±0.06(n=10)$^{\$\$}$	0.75±0.10 (n=15)$^{\$\$}$	0.88±0.13 (n=12)$^{\$\$}$
FECa	1.9±0.3 (n=11)	1.5±0.2 (n=13)	1.4±0.2 (n=12)	2.9±0.3 (n=10)$^{\$}$	3.1±0.3 (n=13)$^{\$\$}$	3.0±0.2 (n=9)$^{\$\$}$
FENa	5.3±0.4 (n=12)	4.7±0.4 (n=13)	5.2±0.5 (n=13)	6.1±0.2 (n=10)	6.1±0.3 (n=15)	6.0±0.3 (n=13)
FEK	0.20±0.004 (n=11)	0.18±0.02(n=13)	0.20±0.01 (n=13)	0.21±0.01 (n=10)	0.23±0.01 (n=15)	0.21±0.01 (n=13)
TmP/GFR	1.6±0.1 (n=9)	1.6±0.1 (n=12)	1.5±0.1 (n=12)	2.0±0.1 (n=10)	1.7±0.1 (n=15)*	1.6±0.1 (n=13)*

Parameters were measured using urine samples obtained over a 24-hour period. Urinary calcium excretion values are shown as μmol/24 hours. Calcium/creatinine ratios (Ca/Cr) are shown as mmol/mmol. Fractional excretion (FE) of Ca and Na are multiplied by 1000. TmP/GFR, ratio of tubular maximum reabsorption of phosphate (TmP) to GFR. All values are expressed as mean ± SEM. A Kruskal-Wallis test followed by Dunn's test for non-parametric pairwise multiple comparisons were used for all analyses. *$p<0.05$ compared to respective *Gna11*$^{+/+}$ mice. $^{\$}p<0.05$, $^{\$\$}p<0.001$ compared to respective male mice.

Table 4. Whole body DXA analysis of *Gna11*$^{+/+}$, *Gna11*$^{+/195G}$ and *Gna11*$^{195G/195G}$ mice

Parameter	**Male**			**Female**		
	Gna11$^{+/+}$	*Gna11*$^{+/195G}$	*Gna11*$^{195G/195G}$	*Gna11*$^{+/+}$	*Gna11*$^{+/195G}$	*Gna11*$^{195G/195G}$
BMC (g)	0.60±0.01 (n=12)	0.62±0.01 (n=13)	0.63±0.01 (n=14)	0.57±0.01 (n=9)	0.59±0.01 (n=14)	0.57±0.01 (n=12)
BMC (corr)	0.02±0.0004 (n=12)	0.02±0.001 (n=13)	0.02±0.001 (n=14)	0.02±0.001 (n=9)	0.02±0.001 (n=15)	0.019±0.001 (n=12)
BMD (g/cm^2)	0.065±0.001 (n=12)	0.065±0.001 (n=13)	0.069±0.002 (n=14)	0.067±0.001 (n=9)	0.066±0.001 (n=15)	0.067±0.003 (n=12)
Fat mass (%)	23.6±0.8 (12)	21.3±1.1 (13)	22.0±1.4 (14)	23.8±1.9 (n=9)	27.4±1.5 (n=15)	29.0±0.7$^{\$}$ (n=12)

DXA, dual-energy X-ray absorptiometry; BMC, bone mineral content; BMC (corr), BMC corrected for body weight; BMD, bone mineral density. All values are expressed as mean ± SEM. A Kruskal-Wallis test followed by Dunn's test for non-parametric pairwise multiple comparisons were used for all analyses. $^{\$}$p=0.06 compared to respective *Gna11*$^{+/+}$ mice.

Table 5. Comparison of the phenotypes of FHH2 patients with mice harboring a loss-of-function *Gna11* mutation.

Parameter	**FHH2 patients**			**FHH2 mouse model**	
	Proband 1	Proband 2	Proband 3	*Gna11*$^{+/195G}$	*Gna11*$^{195G/195G}$
$G\alpha_{11}$ mutation	Leu135Gln (Het)	Ile200del (Het)	Thr54Met (Het)	Asp195Gly (Het)	Asp195Gly (Hom)
Serum/plasma biochemistry					
Calcium	↑	↑	↑	↑	↑
Magnesium	N	↑	nr	N	N
Phosphate	N	N	N	N	↓
Creatinine	N	N	N	N	N
ALP	N	N	nr	N	↑[a]
PTH	N	N	N	N	↑
TSH[b]	N	nr	nr	nr	nr
Urine biochemistry					
FECa	↓[c]	N	N	N	N
Infertility[b]	nr	No	nr	No	nr
Reference	Nesbit et al. 2013 (3)	Nesbit et al. 2013 (3)	Gorvin et al. 2016 (10)	-	-

[a]Alkaline phosphatase (ALP) is increased in homozygous females; [b]Thyrotropin (TSH) reported as 4.05 mU/L (normal 0.35-5.5) (3). Thyrotropin-releasing hormone receptor (TRHR) and gonadotropin-releasing hormone receptor (GnRHR), which are both GPCRs signal via $G\alpha_{11/q}$ proteins (40). However, FHH2 patients with $G\alpha_{11}$ loss-of-function mutations have not been reported to have hypothyroidism, high circulating TSH concentrations (3), or infertility (3, 41), indicating that they are unlikely to have thyroid hormone or gonadotropin hormone deficiencies. The findings of normal body weights in mutant *Gna11*$^{+/195G}$ and *Gna11*$^{195G/195G}$ mice (Table 2) and fertility in mutant *Gna11*$^{+/195G}$ mice (Table 1), suggests that these *Gna11* mutant mice, similar to the FHH2 patients, are also unlikely to have deficiencies of thyroid hormone or gonadotropin hormone. [c]Fractional excretion of calcium (FECa) is <0.01, consistent with the phenotype of FHH. Het, heterozygous; Hom; homozygous; N, normal; PTH, parathyroid hormone; ↑,high; ↓ low; nr, not reported.

Figure 1

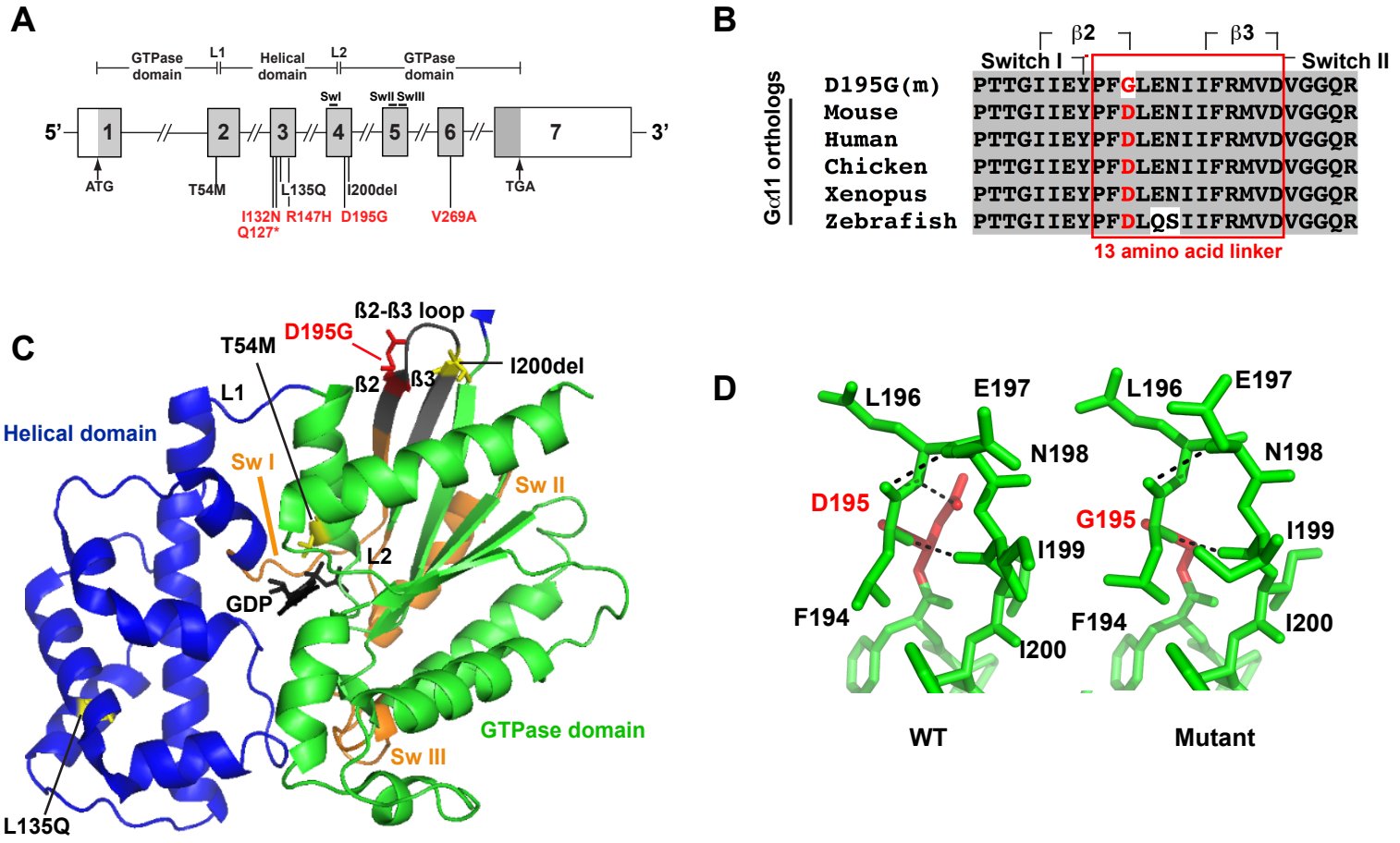

Figure 1. Structural characterization of the Asp195Gly Gα$_{11}$ mutation. (**A**) Genomic organization of *Gna11* showing the location of reported human familial hypocalciuric hypercalcemia type 2 (FHH2) mutations (black) (3, 10) and *Gna11* variants identified in *N*-ethyl-*N*-nitrosourea (ENU)-mutagenized mice (red). The G-protein subunit α$_{11}$ (G α$_{11}$ GTPase domain (encoded by exon 1, 5′ portion of exon 2, 3′ portion of exon 4 and exons 5–7) is connected to the helical domain (encoded by the 3′ portion of exon 2, exon 3, and 5′ portion of exon 4) by the linker 1 (L1) and 2 (L2) peptides. The GTPase domain contains three flexible regions, termed switch regions I-III (SwI-SwIII). The Asp195Gly mutation is located within the GTPase domain, and between the switch I and II regions. (**B**) Multiple protein sequence alignment of Gα$_{11}$ residues comprising a 13 amino acid region that links the β2 strand of the switch I region with the β3 strand of the switch II region. Conserved residues are shown in gray. The WT (Asp, D) and mutant (m) (Gly, G) residues are shown in red. (**C**) Homology model of the GDP-bound Gα$_{11}$ protein. The Gα helical (blue) and GTPase (green) domains, and bound GDP nucleotide (black) are shown. Switch regions I-III are shown in orange. Previously reported residues mutated in FHH2 patients (3, 10) are shown in yellow. The mutated Asp195 residue (red) is located in a 13 amino acid region (gray) and adjacent to the β2-β3 loop. (**D**) Close-up view the β2-β3 hairpin loop region of WT and mutant Gα$_{11}$ proteins showing the structural effects of the Asp195Gly mutant on hydrogen bonds (broken lines) within the hairpin loop. The Asp195Gly Gα$_{11}$ mutant is predicted to result in a loss of a polar contact (hydrogen bond) between the Asp195 side chain and the backbone of the Glu197 (E197) residue. The one-letter amino acid codes indicate D – aspartic acid, E – glutamic acid, F – phenylalanine, G – glycine, I – isoleucine, L – leucine, M – methionine, N – asparagine, Q – glutamine, and T - threonine.

Figure 2

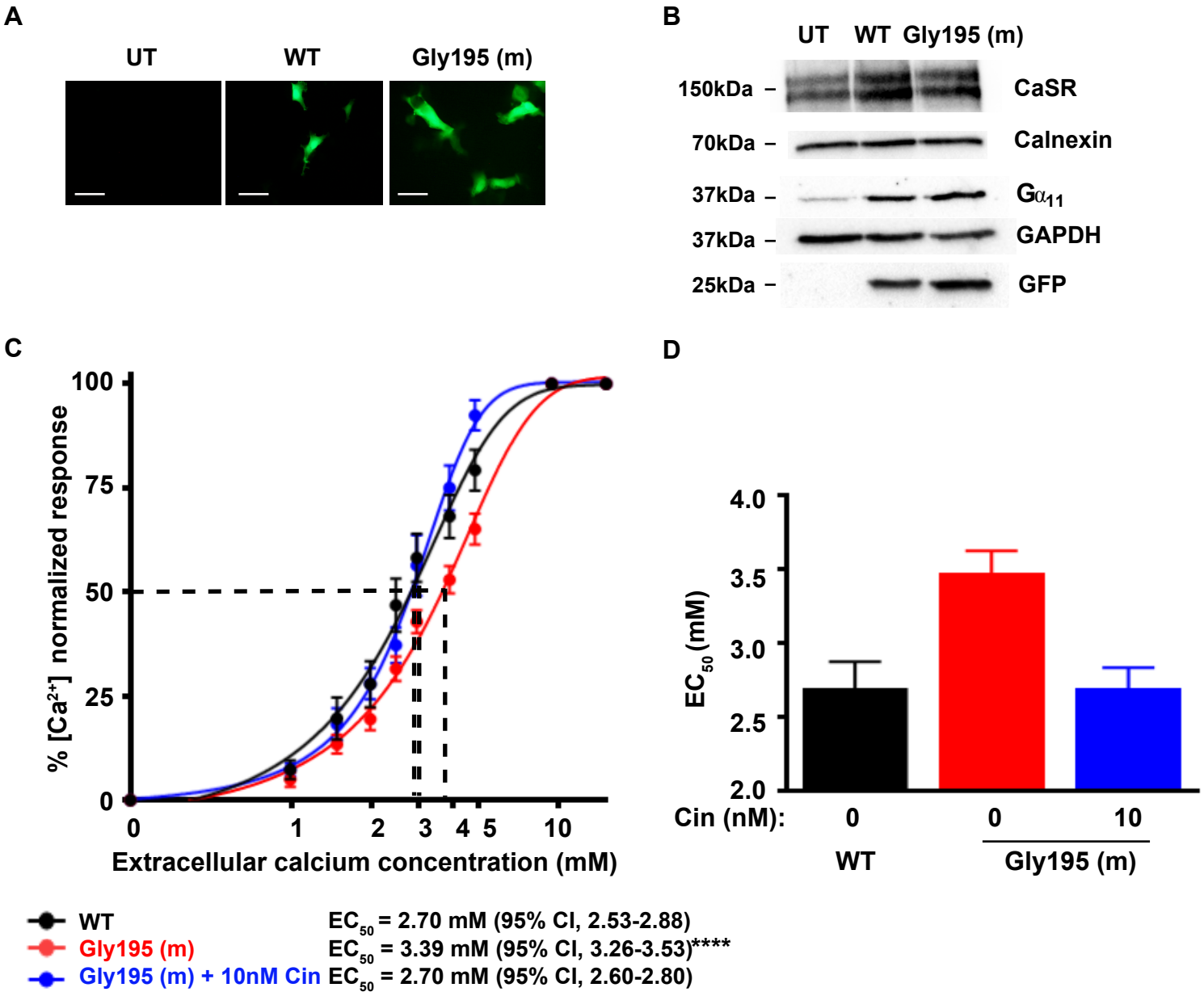

Figure 2. $Ca^{2+}{}_i$ responses of the Gly195 $G\alpha_{11}$ mutant and *in vitro* effect of cinacalcet treatment. (**A**) Fluorescence microscopy of untransfected (UT) HEK293 cells stably expressing calcium-sensing receptor (CaSR) (HEK-CaSR), and of HEK-CaSR cells transiently transfected with WT (Asp195) or mutant (m) Gly195 pBI-CMV2-*GNA11-GFP* constructs. GFP expression in these cells indicates successful transfection and expression by these constructs. Bar indicates 10μm. (**B**) Western blot analysis of lysates from HEK-CaSR cells used for intracellular calcium ($Ca^{2+}{}_i$) experiments. Transient transfection with WT or mutant Gly195 G-protein subunit α_{11} ($G\alpha_{11}$) expression constructs resulted in overexpression of $G\alpha_{11}$ and GFP, whereas untransfected cells showed only endogenous $G\alpha_{11}$ protein expression. All cells expressed the CaSR. The calnexin and GAPDH proteins were used as loading controls. (**C**) $Ca^{2+}{}_i$ responses to changes in $[Ca^{2+}]_o$ of HEK-CaSR cells expressing WT or Gly195 $G\alpha_{11}$ mutant proteins. The $Ca^{2+}{}_i$ responses are expressed as a percentage of the maximum normalized responses and shown as the mean±SEM of 8 independent transfections. The Gly195 $G\alpha_{11}$ mutant led to a rightward shift in the concentration-response curve (red line) compared to cells expressing WT $G\alpha_{11}$ (black line). The addition of 10nM cinacalcet (Cin) normalized the shift of the mutant concentration-response curve (blue line) (**D**) Histogram showing the mean half-maximal concentration (EC_{50}) with 95% confidence intervals (CI) of WT cells (black), Gly195 mutant cells (red), and Gly195 mutant cells treated with 10 nM cinacalcet (blue). Statistical analysis was performed using the F-test. ****p<0.0001 compared to WT.

Figure 3

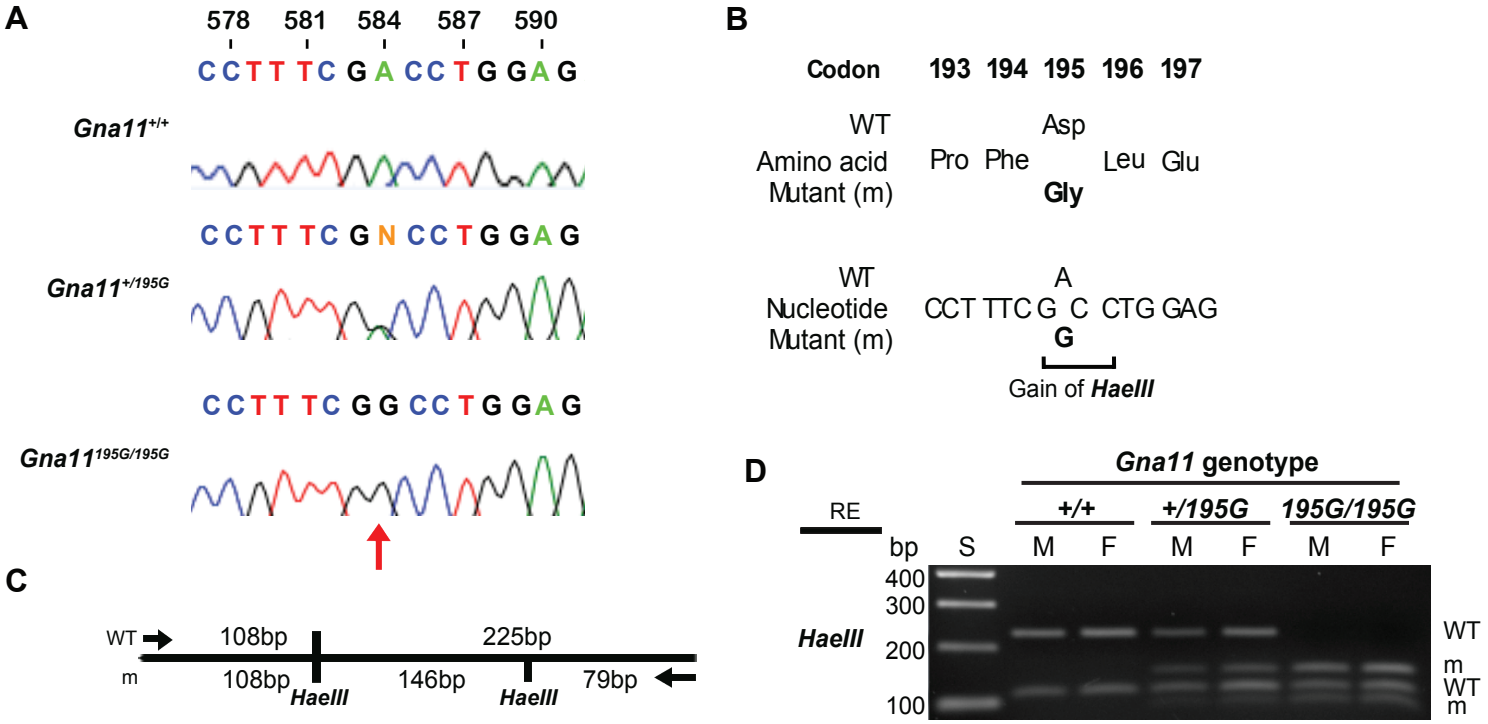

Figure 3. DNA sequence and restriction endonuclease analysis of the Asp195Gly Gα$_{11}$ mutation. (**A**) DNA sequence analysis showing an A-to-G transition at c.584 (red arrow) within exon 3 of *Gna11*. The DNA sequence chromatograms show that WT (*Gna11*$^{+/+}$) mice are homozygous A/A, the heterozygous mutant *Gna11*$^{+/195G}$ mice are A/G, and the homozygous mutant *Gna11*$^{195G/195G}$ mice are G/G. (**B**) This A to G transition was predicted to lead to a missense substitution of Asp, encoded by GAC, to Gly, encoded by GGC, at codon 195, and resulted in the gain of a *HaeIII* restriction endonuclease (RE) site (GG/CC). (**C**) Restriction maps showing that *HaeIII* digest would result in two products of 108bp and 225bp for the WT, and three products of 108bp, 146bp and 79bp for the mutant (m). (**D**) RE digest of *Gna11* exon 3 PCR products demonstrating that WT (*Gna11*$^{+/+}$) mice are homozygous for the WT alleles, mutant *Gna11*$^{+/195G}$ mice are heterozygous and have WT and m alleles, and mutant *Gna11*$^{195G/195G}$ mice are homozygous for m alleles. M = male; F = female; S = size marker.

Figure 4

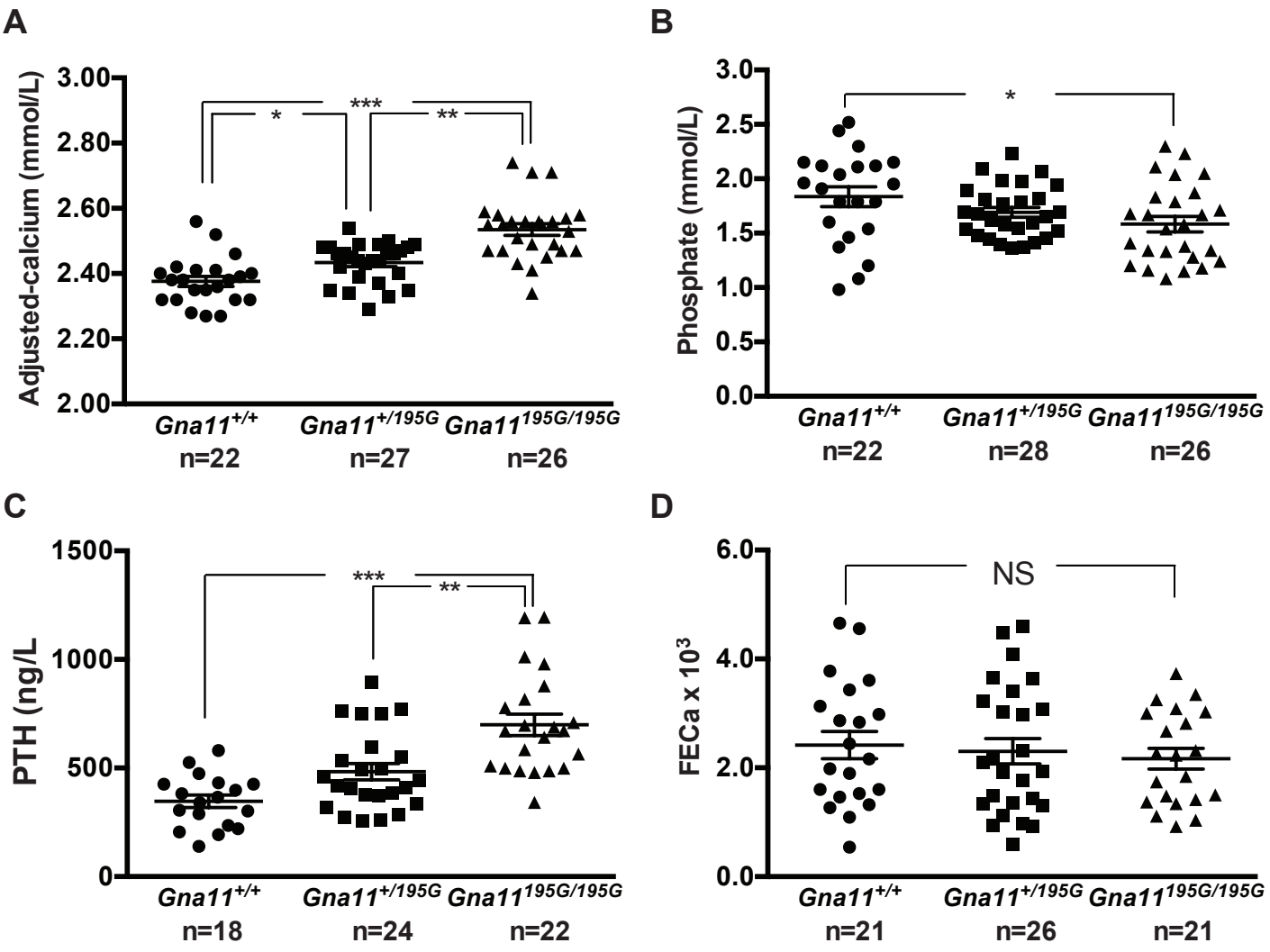

Figure 4. Calcitropic phenotype of *Gna11*$^{+/+}$, *Gna11*$^{+/195G}$ and *Gna11*$^{195G/195G}$ mice. (A) Plasma albumin-adjusted calcium concentrations, (B) plasma phosphate concentrations, (C) plasma parathyroid hormone (PTH) concentrations, and (D) fractional excretion of calcium (FECa) of *Gna11*$^{+/+}$ (circles), *Gna11*$^{+/195G}$ (squares) and *Gna11*$^{195G/195G}$ (triangles) mice, respectively. Combined data from males and females are shown. Mean ± SEM values for the respective groups are indicated by the solid bars. A Kruskal-Wallis test followed by Dunn's test for non-parametric pairwise multiple comparisons were used for analysis of A-D. *p<0.05, **p<0·01. ***p<0.001. NS, non-significant.

Figure 5

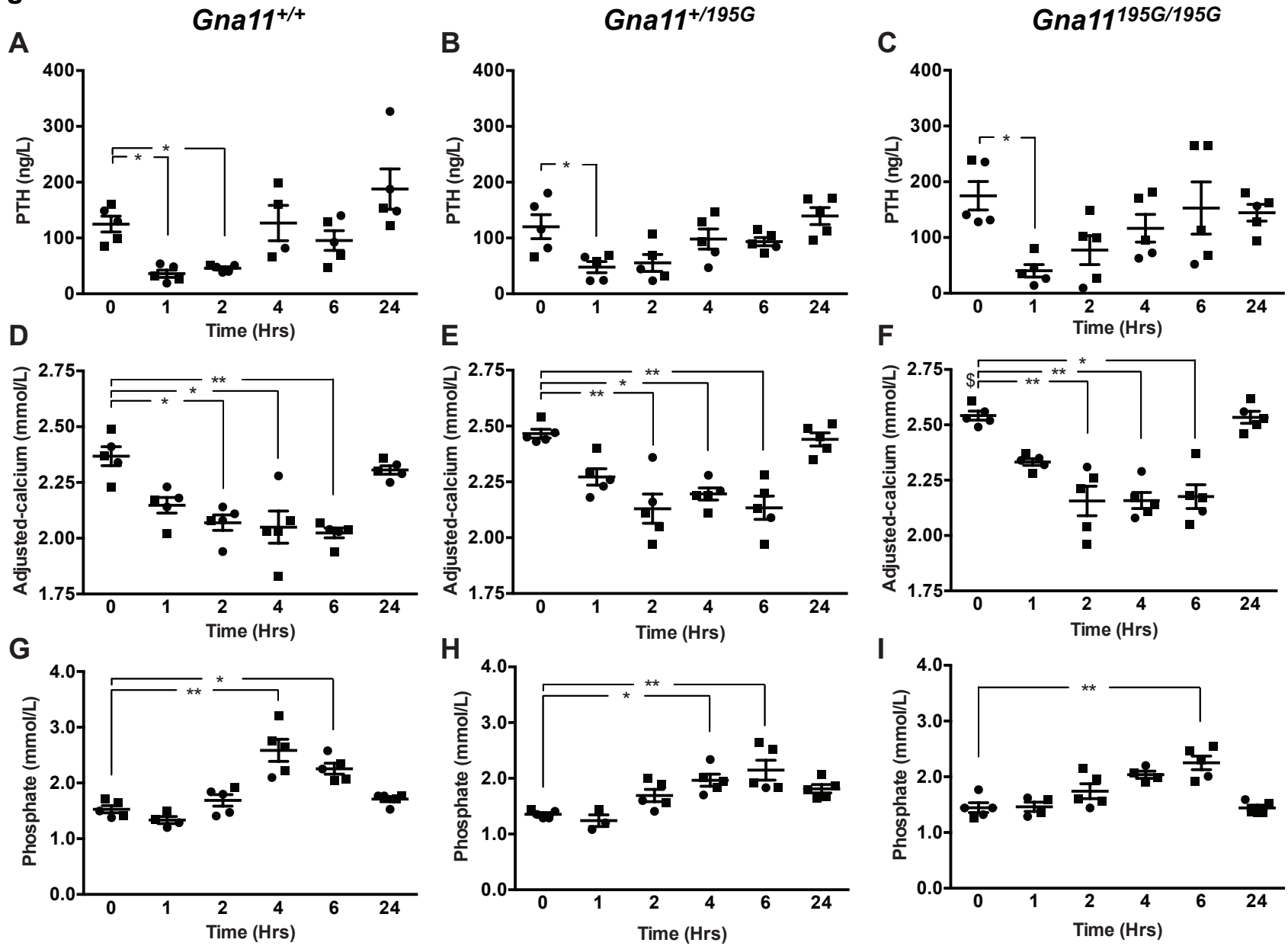

Figure 5. *In vivo* effect of cinacalcet on plasma PTH, calcium and phosphate concentrations of *Gna11*$^{+/+}$, *Gna11*$^{+/195G}$ and *Gna11*$^{195G/195G}$ mice. (**A-C**) Plasma parathyroid hormone (PTH), (**D-F**) plasma albumin-adjusted calcium, and (**G-I**) plasma phosphate concentrations are shown at 0, 1, 2, 4, 6 and 24h following oral gavage administration of a single 30mg/kg cinacalcet dose. Mean values for the respective groups are indicated by solid bars. N=4-5 mice per study time-point. Squares, males; circles, females. A Kruskal-Wallis test followed by Dunn's test for non-parametric pairwise multiple comparisons were used for analysis of A-I. *p<0.05, **p<0·01 compared to respective untreated mice. $^{\$}$Untreated *Gna11*$^{195G/195G}$ mice were significantly (p<0.05) hypercalcemic compared to untreated *Gna11*$^{+/+}$ mice.